García Trenco, A.; Martinez Feliu, A. (2014). The influence of zeolite surface-aluminum species on the deactivationof CuZnAl/zeolite hybrid catalysts for the direct DME synthesis. Catalysis Today. 227:144-153. doi:10.1016/j.cattod.2013.09.051.

A rational strategy for preparing Cu-ZnO/H-ZSM-5 hybrid catalysts with enhanced stability during the one-step conversion of syngas to dimethyl ether (DME)

Andrés García-Trenco, Agustín Martínez*

Instituto de Tecnología Química, CSIC-UPV, Avda. de los Naranjos s/n, 46022 Valencia, Spain

*Corresponding author. Phone: +34 963 877 808. Fax: +34 963 877 809. *E-mail address:* amart@itq.upv.es.

Abstract

In this work, an original approach for preparing Cu-ZnO+H-ZSM-5 (Si/Al=15, denoted as Z5) hybrid catalysts displaying enhanced stability during the direct DME synthesis from syngas is presented. The adopted preparation strategy was based on the effective confinement of the copper catalyst within the pores of an SBA-15 silica carrier (d_{pore}= 7.0 nm) prior to mixing with the acid zeolite. In order to maximize the Cu-ZnO interface area (where active Cu^0 sites are likely located) the walls of the SBA-15 silica were coated with a near-monolayer of ZnO (17 wt% Zn) prior the incorporation of copper (in concentrations of 10, 15, and 20 wt%) by the so-called ammonia-driving deposition-precipitation (ADP) method. Copper nanoparticles sizing 5-6 nm after H_2-reduction (HRTEM) were effectively confined inside the SBA-15 mesopores (as supported by HAADF-STEM) for Cu loadings of up to 15 wt%. Higher Cu loadings (20 wt%) lead to large, XRD-visible, CuO nanoparticles residing out of the SBA-15 pores. The confined catalyst loaded with 15 wt% Cu (15Cu/Zn@S15) displayed the highest Cu^0 surface area (determined by N_2O-RFC) and methanol synthesis activity. Then, hybrid catalysts based on this methanol synthesis function (15Cu/Zn@S15+Z5) were prepared in a 15Cu/Zn@S15:Z5 mass ratio of 2:1 by two methods: a) grinding the mixture of powders prior to pelletizing (method G), and b) mixing the pre-pelletized components (method M). Equivalent hybrids comprising a conventional coprecipitated Cu-ZnO-Al_2O_3 (CZA) catalyst were also prepared for comparative purposes (CZA+Z5). The catalysts were evaluated for direct DME synthesis (533 K, 4.0 MPa) in runs lasting ca. 24 h. It was found that the confined 15Cu/Zn@S15+Z5 hybrids deactivated at a much lower rate than those based on CZA regardless the method of preparation. In turn, while conventional CZA+Z5 catalysts prepared by grinding (G) experienced a higher deactivation than that obtained by mixing (M) due to the contribution of detrimental interactions between the copper and zeolite components in the former, no differences in the deactivation rate were observed for the 15Cu/Zn@S15+Z5 hybrids prepared by grinding and mixing. The improved stability of these hybrid catalysts is accounted for by the inhibition of both detrimental interactions (by avoiding the direct contact of copper active sites and the zeolite surface) and extensive metal sintering (by limiting the extent of Cu^0 crystal growth) induced by the effective confinement of the Cu-based catalyst within the SBA-15 pores.

Keywords: Synthesis gas; direct DME synthesis; hybrid catalysts; confined Cu-ZnO methanol synthesis catalyst; SBA-15 silica support; H-ZSM-5; deactivation; copper sintering; detrimental interactions.

1. INTRODUCTION

Ultra-clean syngas-derived fuels (usually referred to as synthetic fuels or synfuels) containing near-zero sulfur and aromatics offer significant environmental benefits over conventional fuels produced by refining of crude oil. As syngas can be obtained from a variety of abundant sources including natural gas, coal, and biomass, an increasing penetration of synthetic fuels in the fuel markets would help in satisfying the raising energy needs while providing a more secure energy supply for non-oil producer countries. In this respect, dimethyl ether (DME) is gaining attractiveness as a synthetic diesel fuel alternative to the conventional oil-derived diesel fuel owing to its high cetane number and clean-burning characteristics [1,2]. This increasing interest has promoted in the last years an intensive research in the so-called direct (or one-step) DME synthesis process (syngas $\rightarrow$ DME) as an economically attractive alternative to the traditional two-step technology (syngas $\rightarrow$ methanol $\rightarrow$ DME). Besides the obvious cost savings related to the reduction in the number of reaction steps, a further advantage of the direct DME synthesis route over the traditional process is the possibility of operating at much higher per-pass CO conversions by overcoming the thermodynamic limitation of the methanol synthesis reaction due to the rapid *in situ* consumption of the methanol formed.

Bifunctional catalysts comprising a Cu-based methanol synthesis function and a solid acid active for methanol dehydration (typically γ- Al_2O_3 or an H-zeolite) are well-suited for the one-step synthesis of DME. Most often, the copper component is a well-optimized co-precipitated Cu-ZnO-Al_2O_3 (CZA) catalyst representative of the high-active catalysts currently employed in modern low-temperature methanol synthesis plants [3]. Regarding the methanol dehydration function, zeolites are generally preferred

over γ-Al_2O_3 because of their stronger acidity allows operation at lower temperatures and, hence, under thermodynamically favorable conditions for the methanol synthesis step. In turn, lower reaction temperatures help in avoiding extensive coking and copper sintering that could jeopardize catalyst activity and lifetime. Furthermore, zeolites are more resistant than γ-Al_2O_3 towards poisoning of acid sites by the water by-product [4,5,6]. Among the zeolites, the medium pore ZSM-5 (MFI) has been by far the most widely applied as the acid component in bifunctional DME synthesis catalysts [5,7,8,9,10,11], though other zeolites such as ferrierite, MCM-22 and its delaminated counterpart ITQ-2, IM-5, and TNU-9 have also been investigated [12,13].

Different strategies have been applied to prepare the bifunctional catalysts for direct DME synthesis. For instance, methods comprising impregnation, co-precipitation, or sol-gel steps (or their combinations) [7,14,15] and even more sophisticated approaches leading to core-shell catalyst structures [16,17,18] have been reported. The most widely applied procedure, however, involves the simple physical mixing of the Cu-based methanol synthesis and acid methanol dehydration components [8,19,20,21,22]. The large number of variables involved in the different preparations and the lack of systematic studies has originated controversy about which method produces the most efficient catalyst. In principle, a better catalytic performance might be expected for preparations favoring a higher degree of intimacy (i.e. shorter contact distance) between the two catalytic functions. According to this concept, catalysts obtained as physical mixtures would be expected to be less active than those prepared by methods involving, for instance, impregnation and/or co-precipitation stages for which a more intimate contact between the two active components is achieved. However, this is not always the case and, in fact, several examples can be found in precedent studies reporting the opposite behavior. For instance, Naik et al. [23]

observed a higher activity for Cu-ZnO-Al_2O_3/SiO_2-Al_2O_3 hybrid catalysts prepared by mechanical mixing with respect to equivalent composites prepared by mixing of the two freshly precipitated catalyst precursors and by co-precipitation methods. These authors attributed the worse catalytic performance of composite catalysts (where both components exist as a single entity) to detrimental interactions between the components arising during catalyst preparation and activation as well as during catalysis [23]. Similarly, Ge et al. [7] did not find a direct relationship between the catalytic activity for direct DME synthesis and the contact separation of the copper and acid sites in a series of bifunctional catalysts prepared by seven different methods. This anomalous behavior was explained, in that case, by a partial coverage of dehydration sites by part of active centers for methanol synthesis as well as to a mutual negative influence between the two functions when they are too close one from each other [7]. The development of detrimental interactions between the two catalytic functions worsening the catalytic performance of bifunctional Cu-ZnO-Al_2O_3/zeolite catalysts during direct DME synthesis has also been demonstrated in our previous studies [13,24]. In these works it was shown that hybrid catalysts prepared as mixtures of pre-pelletized components are more active and stable than those obtained by the widely applied method of grinding the two component powders followed by pelletizing the homogeneous powder mixture, despite a closer contact between components is attained with the later approach. Our studies revealed that when the reaction is run under kinetic control by the methanol synthesis step (i.e. with an "excess" of dehydration sites), such detrimental interactions lead to a gradual decline of the activity of the Cu-based catalyst, and hence of DME yield, with time-on-stream (TOS). The extent by which this particular mode of deactivation in hybrids prepared by grinding occurs was seen to depend mainly and conjointly on two zeolite parameters, namely the external surface

area (related to the zeolite topology and morphology/size of the crystallites), and the concentration of surface extraframework (EFAL) species [25]. Although the precise mechanism through which the detrimental interactions take place still remains unclear, a water-assisted surface diffusion of mobile EFAL species from the external zeolite surface to the Cu catalyst at the surface contact between CZA and zeolite particles has been hypothesized as the likely cause for the gradual poisoning of active Cu sites [25].

It is clear from the above discussions that adverse interactions between the two types of active sites should be avoided (or minimized) in order to produce more efficient bifunctional zeolite-based catalysts for direct DME synthesis. To this purpose, in the present work we report a rational approach for preparing hybrid catalysts based on the confinement of a Cu-ZnO methanol synthesis function inside the pores of the ordered mesoporous SBA-15 silica host prior to mixing with H-ZSM-5 zeolite used as the dehydration component. Confinement on the Cu-based catalyst inside the SBA-15 pores is expected to avoid the direct contact of the active Cu sites with the zeolite surface and, hence, the development of detrimental interactions, as well as to inhibit Cu sintering during catalysis, a common source of deactivation in industrial Cu-based methanol synthesis catalysts [26].

2. EXPERIMENTAL

2.1. Synthesis of SBA-15 silica and Cu/Zn@SBA-15 methanol synthesis catalysts

The mesoporous SBA-15 silica host was synthesized following the procedure originally reported by Zhao et al. [27]. In short, the triblock copolymer Pluronic P123 (Aldrich) was first dissolved in an aqueous solution of HCl (37 wt%, Scharlab) at 308 K and then tetraethyl orthosilicate (TEOS, Merck) was added dropwise to the above

solution to form a gel with the following molar composition: $1SiO_2$:0.012P123:5.85HCl:204.86H_2O. The resulting suspension was stirred at 308 K for 20 h and hydrothermally treated in a Teflon-lined autoclave at 363 K for 24 h. The obtained solid was filtered, extensively washed with deionized water, dried, and finally air-calcined at 773 K for 16 h.

A series of Cu/Zn@SBA-15 methanol synthesis catalysts were prepared by sequential incorporation of Zn and Cu precursors as follows. First, Zn was incorporated to the SBA-15 silica by incipient wetness impregnation using an aqueous solution of $Zn(NO_3)_2 \cdot 6H_2O$ (≥99%, Aldrich), followed by drying at 373 K for 12 h and calcination at 623 K for 4 h in flowing air. The concentration of the Zn precursor in the impregnating solution was purposely adjusted to target a Zn loading of 17 wt%. This loading roughly corresponds to a theoretical monolayer of ZnO assuming that each Zn^{2+} is bonded to the SBA-15 surface by two oxygen atoms of surface Si-OH groups and a surface density of four Si-OH/nm^2 in the SBA-15 silica [28]. This sample is denoted as Zn@S15. Subsequent loading of copper over the Zn@S15 carrier is anticipated to maximize the Cu-ZnO interface area where active Cu sites are believed to be located. The incorporation of Cu was achieved by the so-called ammonia-driving deposition-precipitation (ADP) [29,30]. In short, $Cu(NO_3)_2$ (Aldrich) was added to an aqueous suspension containing the calcined Zn@S15 carrier in the required amounts to obtain nominal Cu loadings of 10, 15, and 20 wt% in the calcined materials. Then, an ammonia aqueous solution (25 wt%) was added to the above suspension so as to attain a Cu/NH_3 molar ratio of 1/4 (initial pH of ca. 11-12). The mixture was stirred at 313 K for 4 h and then heated to 353 K until complete evaporation of the solvent. Finally, the solid was dried at 373 K overnight and air-calcined at 823 K for 4 h. These catalysts are abbreviated as *x*Cu/Zn@S15, where *x* stands for the nominal Cu loading.

For comparison purposes, a conventional ternary Cu-ZnO-Al_2O_3 methanol synthesis catalyst (Cu:Zn:Al atomic ratio of 55:30:15, abbreviated as CZA) was prepared by coprecipitation of an aqueous solution containing the respective metal nitrates at 343 K and constant pH of 7 using Na_2CO_3 as precipitating agent [31]. The precipitate was separated by filtration, exhaustively dried with deionized water, dried at 373 K overnight, and finally calcined at 673 K for 4 h under flowing air.

2.2. Preparation of hybrid catalysts

Bifunctional hybrid catalysts for direct DME synthesis were prepared as physical mixtures of the methanol synthesis catalyst and a commercial H-ZSM-5 zeolite (Si/Al= 15, CBV3020, Zeolyst Int., abbreviated as Z5) as methanol dehydration function. A mass ratio of 2 between the methanol synthesis and methanol dehydration components was employed for all the hybrids used in the present study with the purpose of running the DME synthesis reaction under kinetic control by the methanol synthesis step. The *x*Cu/Zn@S15 sample giving the highest methanol synthesis activity (as assessed in independent methanol synthesis experiments, see section 2.4) was used as the methanol synthesis component in the formulation of the hybrid catalysts. In order to decouple the contribution of detrimentral interactions to the deactivation of the Cu-based catalyst from other mechanisms (i.e. Cu sintering, carbon deposition), two methods of combining the Cu-based and zeolite components in the hybrids were adopted: a) carefully grinding the powders of the two components in an agate mortar followed by pelletizing the homogeneous powder mixture to 0.25-0.42 mm pellet size (method G), and b) physically mixing the pre-pelletized (0.25-0.42 mm) components (method M). The latter method minimizes the surface contact between the particles of

methanol synthesis catalyst and zeolite preventing the development of detrimental interactions [13,22,24]. The hybrid catalysts prepared by methods G and M are denoted as MSC+Z5(G) and MSC+Z5(M), respectively, where MSC stands for the nomenclature specifically employed for the methanol synthesis catalyst as described in the previous section.

2.3. Characterization techniques

The chemical composition of the methanol synthesis catalysts and the Si/Al ratio of the H-ZSM-5 zeolite was determined by Inductively Coupled Plasma-Optical Emission Spectroscopy (ICP-OES) in a Varian 715-ES apparatus after dissolution of the solids in an acid mixture of 20%HNO_3:20%HF:60%HCl (vol%).

Crystalline phases in the materials were identified by powder X-ray diffraction (XRD) in a Panalytical Cubix Pro diffractometer equipped with a graphite monochromator operating at 40 kV and 45 mA using nickel-filtered CuK_α radiation (λ= 0.1542 nm). Hydrogen-reduced and spent catalysts were carefully withdrawn from the reactor and rapidly stored under inert atmosphere until being transferred to the sample holder of the diffractometer. The average crystallite size of the CuO and Cu^0 phases were estimated by applying the Scherrer's equation to the most intense peak at 38.8º and 43.3º (2θ), respectively, after background subtraction and correction for instrumental broadening. Additionally, low angle X-ray diffraction measurements were performed for selected samples in a PANanalytical X'Pert PRO diffractometer using CuK_α radiation.

FTIR spectra of Zn@S15 and S15 samples were recorded in a Nicolet 710 equipment for self-supported wafers of 10 mg/cm^2. Prior to the measurements, the samples were outgassed overnight at 473 K under dynamic vacuum of 10^{-2} Pa.

Textural properties of the samples (ca. 200 mg) were derived from the respective N_2 adsorption-desorption isotherms recorded at 77 K on an ASAP-2000 (Micromeritics) equipment after pretreatment at 673 K and vacuum overnight. Specific surface areas were obtained by the BET method, and pore size distributions were derived from the adsorption branches of isotherms by using the Barrett-Joyner-Halenda (BJH) model.

The reduction behavior of the calcined methanol synthesis catalysts was assessed by H_2-TPR in a Micromeritics Autochem 2910 equipment. About 50 mg of sample was flushed at room temperature (RT) for 0.5 h with the reductive gas mixture of 10 vol% H_2 in Ar and then the temperature was linearly increased from RT to 1073 K at a heating rate of 10 K/min. A 2-propanol/N_2(l) trap was used to retain water formed during the reduction while the H_2 consumption rate was continuously monitored in a thermal conductivity detector (TCD) previously calibrated using the reduction of CuO as reference.

Copper surface areas in selected as-reduced and spent hybrid catalysts were obtained by the N_2O-RFC ("reactive frontal chromatography") method [32]. Measurements were performed in an Autochem II (Micromeritics) equipment coupled with a quadrupole mass spectrometer (OmniStar from Balzers Instruments). First, about 100 mg of calcined precursor (0.25-0.42 mm pellet size) were reduced by flowing a 10%H_2/Ar gas mixture at 750 K for 1 h (for Cu/Zn@S15 samples) or at 518 K for 10 h (for CZA). Subsequently, a flow of 10 cm^3·min^{-1} of the reactive 2% N_2O/He gas mixture was passed through the catalyst at 333 K until no changes in the monitored

m/z= 44 (N_2O) and m/z= 28 signals (N_2) were evidenced. Copper surface areas were calculated from the amount of N_2O reacted considering a reaction stoichiometry of N_2O:Cu of 1:2 and an atomic copper surface density of $1.46 \cdot 10^{19}$ Cu atoms/m^2 [33].

High Angle Annular Dark Field-Scanning Transmission Electron Microscopy (HAADF-STEM) and High-Resolution (HR) TEM images were recorded on a 200 kV JEOL JEM-2010F instrument using an electron beam probe of 0.5 nm of diameter at a diffraction camera length of 10 cm. Chemical composition analysis using line spectrum measurements were performed at the nanometric scale by X-ray energy-dispersive spectroscopy (EDX) using an Oxford INCA Energy 2000 system coupled to the microscope.

The amount of carbon deposits in spent catalysts was determined by elemental analysis (EA) in a EA1108 CHNS-O analyzer (Fisons Inst.). Furthermore, the reactivity of the formed carbon species towards oxidation was assessed by temperature-programmed oxidation (TPO) in the same equipment described above for the N_2O-RFC characterization. Prior to the measurements, a flow of He was passed through the spent sample (ca. 130 mg) at 573 K for 30 min (10 K/min) to remove physically adsorbed species. Then, the sample was cooled down to 373 K and flushed with a gas mixture comprising 5 vol% O_2 in He, and the temperature linearly increased at a heating rate of 5ºC/min up to 1073 K. The evolution of the gaseous species with m/z= 44, 28, and 18 corresponding to CO_2, CO, and H_2O, respectively, was monitored in the mass spectrometer to determine the combustion profiles.

2.4. Catalytic experiments

Syngas-to-methanol (STM) and syngas-to-DME (STD) experiments were performed in a down-flow fixed bed tubular reactor. Typically, the reactor was loaded with 1.0 g of catalyst (0.25-0.42 mm pellet size) previously diluted with the required amount of inert SiC particles (0.6-0.8 mm) to achieve a total bed volume of 10 cm^3. Prior to reaction, the catalysts were reduced *in situ* in flowing H_2 (5 vol% H_2 in N_2) at atmospheric pressure. The conventional CZA and CZA+Z5 hybrids were reduced at 518 K for 10 h while those based on Cu/Zn@SBA-15 were reduced at 750 K for 1 h as the later reduction conditions were reported to maximize the activity for methanol synthesis of silica-supported Cu/ZnO catalysts [34,35,36]. Both methanol synthesis and direct DME synthesis experiments were carried out at 533 K and 4.0 MPa feeding a gas mixture of 90 vol% syngas (66%H_2/30%CO/4%CO_2, vol%) and 10 vol% Ar (used as internal standard for GC analyses). The space velocity in methanol synthesis experiments was adjusted to obtain initial CO conversions below 10% (differential conditions). For direct DME synthesis, the space velocity was adjusted in each catalyst so as to obtain initial CO conversions of ca. 60-75% in runs lasting ca. 24 h. Control experiments indicated the absence of internal and external mass transfer limitations under the reaction conditions employed in both methanol and DME synthesis experiments. The product stream exiting the reactor was analyzed on line by gas chromatography in a Varian 450-GC equipped with two packed columns (13X Molecular Sieve and Porapak HaysepQ) and one capillary column (CP-Sil 5 CB) and two detectors (TCD and FID). Product selectivities are given on a carbon basis, taking into account the amount of CO_2 already present in the syngas feed. Carbon mass balances of 100 ± 2% were obtained for the reported experiments.

3. RESULTS AND DISCUSSION

3.1. Characterization of materials

The physicochemical properties of the calcined and H_2-reduced reference CZA catalyst have been reported elsewhere [30] and summarized in Table S1 of Supporting Information. These properties are consistent with reported values for an equivalent coprecipitated Cu-ZnO-Al_2O_3 catalyst [31].

The chemical composition and textural properties for the calcined SBA-15 silica (S15), ZnO@SBA-15 composite (Zn@S15), and Cu/ZnO@SBA-15 catalysts (*x*Cu/Zn@S15) are shown in Table 1. The Zn content in the Zn@S15 sample (16.9 wt%) perfectly matched the nominal value of 17 wt% expected from the concentration of Zn precursor in the impregnating solution (see section 2.1). As shown in Fig. S1 of Supporting Information, the intensity of the IR band at 3742 cm^{-1} of isolated silanol groups in SBA-15 was largely reduced upon impregnation with $Zn(NO_3)_2$ and subsequent calcination. This result indicates that most of the silanol groups were reacted with the Zn precursor and/or covered by ZnO species. The isolated silanols remaining upon incorporation of ZnO may be due to unreacted and/or uncovered regions on the SBA-15 surface and probably also to the contribution of inaccessible Si-OH groups buried in the silica walls [37]. On the other hand, the experimental Zn and Cu contents in the calcined Cu/Zn@SBA-15 materials did also concur with the nominal values.

The N_2 adsorption-desorption isotherms and the corresponding pore size distributions for the S15, Zn@S15, and *x*Cu/Zn@S15 samples are shown in Figs. 1a and 1b, respectively. Both the silica support and the metal loaded samples displayed type IV adsorption isotherms with H1-type hysteresis loop (Fig. 1a) typical of the SBA-15 material, indicating that the porous structure of the carrier was largely preserved upon metal incorporation. The pore size distributions are relatively narrow and centered at

around 7.0 nm in the pristine S15 carrier and at ca. 6.5 nm in the metal-loaded samples (Fig. 1b). On the other hand, a decrease in the total N_2 uptake with respect to the S15 carrier was evident in Fig. 1a for Zn@S15 and *x*Cu/Zn@S15 samples. As seen in Table 1, the BET area and mesopore volume of the SBA-15 host were, respectively, 771 m^2/g and 0.93 cm^3/g. Both textural parameters decreased upon loading of Zn and Cu, the decrease being more pronounced with the increase in copper content. This decrease in textural properties can be partly ascribed to the mass-dilution effect caused by the metal oxide phases. Correcting the mesopore volumes per mass of SBA-15 silica (that is, considering the mass-dilution effect) results in relative decreases of, respectively, 10% and ca. 20% for Zn@S15 and *x*Cu@Zn/S15 samples (Table 1) which suggests a partial plugging of the mesopores by the confined metal oxide phases.

Low-angle XRD patterns for S15, Zn@S15, and 15Cu/Zn@S15 samples (Fig. 2a) reveal the (100), (110), and (200) reflections attributed to the hexagonal arrangement of SBA-15 mesopores, further confirming the preservation of the SBA-15 pore structure in the metal-loaded samples. A slight decrease in the intensity of the (100) reflection with respect to the SBA-15 carrier can be noticed, however, for Zn@S15 and 15Cu/Zn@S15 which may be related with a reduced scattering contrast between the silica walls and the inner space by the occluded metal oxide species. Nonetheless, a certain reduction in the long-range periodicity order of the mesopores cannot be discarded. The high-angle XRD patterns for the metal-containing calcined precursors are presented in Fig. 2b. The lack of reflections related to ZnO is indicative of a high dispersion of the Zn species on the SBA-15 surface. Indeed, previous studies have shown the occurrence of a strong interaction between ZnO_x species and the siliceous matrix leading to an amorphous bi-dimensional zinc silicate layer and preventing the formation of ZnO aggregates even at coverages exceeding the monolayer

[37,38]. As also seen in Fig. 2b, no reflections related to CuO crystallites (JCPDS 80-1268) were perceived for the calcined *x*Cu/Zn@S15 samples with Cu loadings of 10 and 15 wt%, indicative of a very high copper dispersion. Conversely, the presence of relatively large CuO crystallites sizing ca. 67 nm in average (as estimated by XRD line broadening analysis) was clearly evidenced in the 20Cu/Zn@S15 sample with the highest Cu content. It is clear that such relatively large CuO particles will be located at the outer surface of the SBA-15 silica matrix.

The reduction behavior of *x*Cu/Zn@S15 catalysts was studied by H_2-TPR. The corresponding reduction profiles are depicted in Fig 3. The H_2-TPR profiles showed a main H_2 consumption feature peaking at temperatures in the 506-520 K range associated to the reduction of CuO species to Cu^0. In fact, the H_2 consumptions associated to this reduction peak concurred well (±3% relative error) with the theoretical values expected from the reduction stoichiometry $CuO + H_2 \rightarrow Cu^0 + H_2O$ and the experimental Cu contents (Table 1). Therefore, it can be presumed that copper will be fully reduced after the in situ reduction treatment at 750 K performed prior the catalytic experiments. It can be also seen in Fig. 3 that all samples presented a minor and broad reduction feature in the high temperature range centered at ca. 865 K which has been assigned to a partial reduction of ZnO species [34,35,39].

The Cu^0 surface areas as determined by N_2O-RFC in the H_2-reduced catalysts are given in Table 1. It can be seen that the total Cu^0 surface area (per mass of catalyst) first raised from 5.7 to 8.7 m^2/g_{cat} with increasing the Cu content from 10 to 15 wt% and then declined to 5.4 m^2/g_{cat} with the further increase in Cu loading to 20 wt%. It is worth noting that both 10Cu/Zn@S15 and 15Cu/Zn@S15 catalysts showed nearly the same Cu^0 surface area per mass of copper (58-60 m^2/g_{Cu}) while this value decreased by about 50% (ca. 27 m^2/g_{Cu}) for sample 20Cu/Zn@S15 reflecting a poorer copper

dispersion in the later, in good agreement with the presence of out-of-pores XRD-visible CuO particles (Fig. 2b).

The location of Cu^0 nanoparticles in the 15Cu/Zn@S15 catalyst after the severe reduction conditions (750 K) applied prior the catalytic experiments was ascertained by electron microscopy. A representative HAADF-STEM image showing the SBA-15 channels partially filled with Cu^0 nanoparticles is presented in Fig. 4a. No large nanoparticles laying at the external surface were observed. The presence of very small Cu^0 nanoparticles (confirmed by EDX) sizing 5-6 nm was clearly evidenced by HRTEM, as exemplified in Fig. 4b. On the other hand, Fig. 4c shows a HAADF-STEM image (left) and the EDX line profile (right) collected along the white line depicted in the HAADF-STEM image. The line profile analysis clearly evidences a maximum concentration of Cu in-between the Si hills (corresponding to the walls of the SBA-15 silica), pointing out to an effective confinement of Cu^0 nanoparticles inside the SBA-15 mesopores. By contrast, the concentration of Zn remained highly homogeneous along the analyzed region, which is consistent with the absence of nanoparticulated ZnO entities and with the formation of a homogeneous bi-dimensional layer on the SBA-15 surface, as discussed previously.

3.2. Catalytic experiments

3.2.1. Selection of methanol synthesis catalyst

First, the catalytic performance of the *x*Cu/Zn@S15 catalysts for methanol synthesis at *pseudo*-differential conditions (CO conversion ≤ 10%) was assessed at the same temperature (533 K) and total pressure (4.0 MPa) employed in direct DME

synthesis experiments (see section 2.4). All the catalysts experienced a similar loss of activity (ca. 30% in relative terms) during the first 5-6 h on stream after which a steady state is reached (see Fig. S2 in Supporting Information). This initial deactivation can be likely ascribed to a certain Cu^0 sintering, as it typically occurs in industrial Cu-ZnO-Al_2O_3 (CZA) methanol synthesis catalysts [26]. The catalytic results are summarized in Table 2. Product selectivities remained almost constant along with the experiments. Methanol was, as expected, the principal reaction product for all catalysts, with selectivities above 91% (on a carbon basis). The rest of products formed comprised CO_2, C_1-C_5 hydrocarbons, C_{2+} alcohols (mainly ethanol), and DME. As seen in Table 2, the methanol synthesis rate (both initial and in the steady state) first increased with increasing the Cu loading from 10 to 15 wt% and then declined at higher Cu contents. Interestingly, the trend in initial synthesis rate roughly parallels that observed for the Cu^0 surface area of the freshly reduced catalysts (Table 1), suggesting that for this series of catalysts the methanol synthesis activity is mainly dictated by the amount of exposed surface Cu^0 sites. A close correlation between the activity for methanol synthesis and the Cu^0 surface area has also been reported for conventional co-precipitated Cu-ZnO-Al_2O_3 catalysts [40,41,42]. Despite the precise nature of the active copper sites and the promoting role of ZnO_x species are still controversial issues [43,44,45,46,47,48], it is generally consented that the active Cu sites are located at the Cu-ZnO_x interface [34,43,49,50,51,52,53]. If this is so, the close parallelism between the activity and copper surface area found in the present study would suggest that a similar extent of Cu promotion by ZnO_x was attained in the *x*Cu/Zn@S15 catalysts, probably as a consequence of the near-monolayer dispersion of ZnO_x on the SBA-15 surface, ensuring a high contact surface between confined Cu^0 nanoparticles and ZnO_x species. Nonetheless, a detailed discussion on this particular issue is out of the scope of the

present investigation. Taking into account the catalytic results shown in Table 2, the most active 15Cu/Zn@S15 catalyst was selected as the methanol synthesis component for the preparation of the hybrid DME synthesis catalysts, as will be discussed in the next section.

3.2.2. Direct DME synthesis on 15Cu/Zn@S15 + H-ZSM-5 hybrid catalysts

Hybrid catalysts were prepared as physical mixtures of the most active 15Cu/Zn@S15 or the reference CZA methanol synthesis catalysts and H-ZSM-5 (Z5) in a 2:1 mass ratio. As detailed in section 2.2, two methods were adopted to prepare the physical mixtures: a) grinding of the two components followed by pelletizing the homogeneous powder mixture (method G), and b) mixing the pre-pelletized components (method M). Direct DME synthesis experiments were performed at 533 K and 4.0 MPa during ca. 24 h on stream. The space velocity (GHSV) was adjusted in each case to obtain initial (at TOS~ 3 h) CO conversions of 60-75% (Fig. S3a). Specifically, a GHSV (referred to the mass of copper) of 3710 and 4640 $cm^3_{syngas}/(g_{Cu}\cdot h)$ was used in the experiments comprising the 15Cu/Zn@S15+Z5 and CZA+Z5 catalysts, respectively. Under these conditions all the hybrid catalysts displayed a similar selectivity pattern: 60-63% DME, 3-4% CH_3OH, 31-34%CO_2, and 2-3% hydrocarbons (% on a carbon basis), although the catalysts based on 15Cu/Zn@S15 were slightly more selective to DME (61-63%) than those based on CZA (58-59%) at equivalent CO conversion (Fig. S3b). These selectivity values approached those predicted by the thermodynamic equilibrium at the studied reaction conditions (68% DME, 5% MeOH, 27% CO_2). This is an indication that there is an "excess" of Brønsted acid sites in the hybrids so as all methanol formed on the Cu-

based catalyst is efficiently dehydrated to DME. Moreover, the selectivity pattern remained constant (within experimental error) during the 24 h runs. The similar and near-equilibrium selectivities obtained indicate, as intended, that the overall DME synthesis process in all the experiments was kinetically controlled by the methanol synthesis step. Thus, any variation in the CO conversion rate with time-on-stream (TOS) could almost exclusively be ascribed to changes in the activity of the Cu-based methanol synthesis component.

Given the markedly different Cu content in the confined 15Cu/Zn@S15 (14.6 wt%, Table 1) and CZA (52.6 wt%, Table S1) methanol synthesis catalysts, the activity for CO conversion of the respective hybrid catalysts during direct DME synthesis is compared in Fig. 5 on a copper mass basis. It can be seen that the catalyst based on CZA prepared by mixing displayed the highest initial (at TOS~ 3 h) CO conversion rate, followed by its equivalent hybrid prepared by grinding. The lower initial activity of the later is likely related to the development of detrimental interactions [13,24]. On the other hand, the initial activity of the hybrids based on the 15Cu/Zn@S15 catalyst was close to that of CZA+Z5(G) and was not influenced by the method of preparation (Fig. 5).

As observed in Fig. 5, all the hybrid catalysts experienced a gradual decline of the CO conversion rate with TOS that reflects a progressive loss of activity of the Cu-based catalyst. For the sake of clarity, the deactivation behavior of the catalysts is compared in Fig. 6 based on normalized CO conversions. It is worth noting that for the hybrid catalysts based on 15Cu/Zn@S15 the deactivation trend was hardly affected by the method of preparation. Conversely, the CZA+Z5 catalyst prepared by grinding (G) deactivated to a larger extent, within the same reaction period, than its counterpart obtained by the mixing method (M). Thus, as shown in Table 3, the relative loss of

activity for CO conversion in the TOS range of 3-24 h was about 11% for both 15Cu/Zn@S15+Z5(M) and 15Cu/Zn@S15+Z5(G) samples while it reached ca. 17% and ca. 27% in the case of CZA+Z5(M) and CZA+Z5(G), respectively.

In general, two main deactivation mechanisms have been proposed in order to account for the loss activity with time of bifunctional catalysts during the one-step DME synthesis process, namely a loss of active Cu^0 sites due to metal sintering [54,55,56,57] and deposition of carbonaceous species [58,59]. In turn, in our previous studies we reported an additional mode of deactivation related to detrimental interactions between the copper and zeolite components in hybrid catalysts presenting a relatively high contact-surface between the two components, such as those prepared by grinding [13,24,25]. Since this deactivation mode did hardly occur in hybrids prepared by mixing the components in the form of pellets (method M) for which the contact-surface between the copper catalyst and zeolite crystallites is minimized [13,24, 25], the loss of CO conversion observed for the catalysts prepared by this method has to be primarily ascribed to metal sintering and/or carbon deposition. Table 3 shows the Cu^0 surface area (per mass of copper) and carbon content measured for the spent hybrid catalysts. The amount of carbon was in all cases low (0.6-1.2 wt%) and showed no obvious correlation with the extent of deactivation. The slightly higher amount of carbon present in spent CZA+Z5 samples (1.0-1.2 wt%) as compared to 15Cu/Zn@S15+Z5 (0.6-0.8%) is most likely attributed to the presence of residual carbonates remaining on the coprecipitated CZA catalyst [40] rather than to carbonaceous species deposited on the metal function, as corroborated by TPO experiments (see high-temperature combustion peaks in Fig. S4 of Supporting Information). In fact, TPO results in Fig. S4 evidenced a low formation of carbon deposits on the metallic function characterized by a low temperature combustion peak at about 500 K [58,59] with no evident correlation with the deactivation trend of

the studied catalysts (Fig. 6). On the other hand, it can be seen in Table 3 that all catalysts underwent a loss of Cu^0 surface area indicative of metal sintering during the catalytic reaction. Interestingly, the relative loss of Cu^0 surface area was lower for the hybrid catalysts comprising the 15Cu/Zn@S15 system (10-12%) in comparison to those based on CZA (17-19%). Moreover, for each type of methanol synthesis component, the relative loss of metal surface area resulted almost independent on the method of preparation (Table 3). The better resistance towards Cu^0 sintering of the 15Cu/Zn@S15 catalyst can be related to the confinement of Cu species inside the SBA-15 mesopores which imposes a steric limitation to the growth of Cu^0 crystallites.

It is worth noting that, for the hybrid catalysts comprising 15Cu/Zn@S15 as the methanol synthesis function and for CZA+Z5(M), there is a good correspondence between the relative loss of Cu^0 surface area after the catalytic reaction and the relative loss of activity (Table 3). In this respect, Sun et al. [60] also found a close correlation between the loss of activity for methanol synthesis and the loss of copper surface area in Cu-ZnO-Al_2O_3 catalysts. Therefore, even if a certain contribution of carbonaceous deposits to the overall deactivation of the hybrid catalysts cannot be completely disregarded, it appears that under the studied conditions sintering of active Cu^0 species in the respective methanol synthesis components is the main source of deactivation in catalysts prepared by method M. In fact, sintering of copper crystallites has been shown to be the only relevant deactivation mechanism in modern Cu-ZnO-Al_2O_3 catalysts under industrial methanol synthesis conditions [26].

As commented before, the conventional CZA+Z5 catalyst prepared by grinding experienced a significantly higher relative loss of CO conversion (26.7%) than that obtained by the mixing method (16.7%) despite the degree of copper sintering (Table 3) as well as the amount and nature of carbon deposits (Table 3 and Fig. S4 of Supporting

Information) was similar for both catalysts. The difference in the extent of deactivation of CZA+Z5(G) and CZA+Z5(M) catalysts can be, thus, attributed to detrimental interactions between the CZA and zeolite components in the former catalyst, in line with our earlier studies [13,24,25]. In the case of 15Cu/Zn@S15+Z5 hybrids, however, there was no practical difference in the deactivation behavior for catalysts prepared by grinding and mixing, as seen in Fig. 6. This result clearly evinces the lack of detrimental interactions in 15Cu/Zn@S15 catalysts irrespective of the method by which the two components are combined.

The above catalytic results unambiguously demonstrate that confinement of the Cu-ZnO methanol synthesis catalyst within the mesopores of SBA-15 silica prior to mixing with the acid zeolite is an effective strategy to avoid the development of detrimental interactions and extensive Cu^0 sintering during the one-step DME synthesis and, consequently, to enhance the stability of hybrid catalysts prepared by the commonly applied method of grinding.

4. CONCLUSIONS

In this work we presented a rational approach for preparing bifunctional Cu-ZnO+H-ZSM-5 hybrid catalysts displaying an improved stability with time during the one-step DME synthesis from syngas. The approach was based on the confinement of the Cu-ZnO methanol synthesis function within the pores of an SBA-15 silica (pore diameter ~ 7 nm). Prior to incorporation of Cu, the SBA-15 silica host was coated with a monolayer of ZnO (sample Zn@S15) in order to maximize the Cu^0-ZnO interface area where the active copper sites for methanol synthesis are presumably located. Then, copper was introduced on the Zn@S15 carrier in concentrations of 10, 15, and 20 wt%

by using the ammonia-driving deposition-precipitation (ADP) method. N_2 physisorption and low-angle XRD measurements revealed that the porous structure of the SBA-15 host was largely preserved upon the incorporation of the metal phases and subsequent calcination. In turn, HAADF-STEM characterization proved that Cu^0 nanoparticles (NPs) in the H_2-reduced catalyst were effectively confined within the SBA-15 pores for Cu loadings of up to 15 wt%, above which large nanoparticles residing on the external surface were detected by XRD. Accordingly, a maximum in the Cu^0 surface area (measured by N_2O-RFC) and methanol synthesis activity (assessed in independent experiments) was obtained for the confined catalyst loaded with 15 wt% Cu (sample 15Cu/Zn@S15). This catalyst was, then, used as the methanol synthesis function in hybrid catalysts comprising zeolite H-ZSM-5 (Si/Al=15, Z5) as the methanol dehydration component in a 15Cu/Zn@S15:Z5 mass ratio of 2:1. For comparative purposes, similar hybrid catalysts were prepared using as methanol synthesis function a conventional coprecipitated CZA catalyst (samples CZA+Z5). Two methods were adopted for preparing the hybrid catalysts: a) grinding the powders prior to pelletizing (method G), and b) mixing the components already in the form of pellets (method M).

When evaluated in the direct DME synthesis (533 K, 4.0 MPa, 24 h TOS), the hybrid catalysts based on the confined 15Cu/Zn@S15 system experienced a much lower deactivation than those based on CZA. Interestingly, while for CZA+Z5 hybrids the catalyst prepared by grinding deactivated to a larger extent than that obtained by mixing due to the contribution of detrimental interactions between the copper function and the zeolite in the former, the deactivation behavior of 15Cu/Zn@S15+Z5 resulted unaffected by the method of preparation. These catalytic trends, in combination with the characterization of spent catalysts by N_2O-RFC (Cu^0 surface area), elemental analysis (carbon content), and TPO (nature and location of carbon deposits), indicated that the

enhanced stability of the hybrid catalysts based on the confined 15Cu/Zn@S15 system during the direct DME synthesis was due to both the avoidance of detrimental interactions and extensive Cu^0 sintering. Thus, on one hand, the effective confinement of the Cu-ZnO function inside the SBA-15 mesopores prevents its direct contact with the external surface of zeolite crystallites which, according to our recent studies, is at the origin of the development of detrimental interactions. On the other hand, the confinement imposes a limit to the growth of Cu^0 crystallites inside the SBA-15 pores, resulting in catalysts that are less prone to sintering under DME synthesis conditions.

In summary, the results reported in the present study demonstrate that confinement of the methanol synthesis function within the pores of the ordered mesoporous SBA-15 silica is an appropriate strategy for improving the stability of hybrid catalysts during the one-step DME synthesis reaction.

Acknowledgements

This research was supported by the Comisión Interministerial de Ciencia y Tecnología (CICYT) of Spain (project CTQ2010-17988/PPQ) and the SEVERO OCHOA Program for Centers of Excellence. The authors are indebted to Dr. J.J. Delgado (Universidad de Cádiz) for the electron microscopy study. A. García-Trenco thanks the Ministerio de Economía y Competitividad of Spain for a predoctoral scholarship.

References

[1] T.A. Semelsberger, R.L. Borup, H.L. Greene, J. Power Sources 156 (2006) 497-511.

[2] N. Inoue, Y. Ohno, Petrotech 24 (2001) 319-322.

[3] K.C. Waugh, Catal. Lett. 142 (2012) 1153-1166.

[4] T. Takeguchi, K. Yanagisawa, T. Inui, M. Inoue, Appl. Catal. 192 (2000) 201-209.

[5] V. Vishwanathan, K.-W. Jun, J.-W. Kim, H.-S. Roh, Appl. Catal. A 276 (2004) 251-255.

[6] M. Xu, J.H. Lunsford, D.W. Goodman, A. Bhattacharyya, Appl. Catal. A 149 (1997) 289-301.

[7] Q. Ge, Y. Huang, F. Qiu, S. Li, Appl. Catal. A 167 (1998) 23-30.

[8] J.-H. Kim, M.J. Park, S.J. Kim, O.-S. Joo, K.-D. Jung, Appl. Catal. A 264 (2004) 37-41.

[9] J. Xia, D. Mao, B. Zhang, Q. Chen, Y. Tang, Catal. Lett. 98 (2004) 235-240.

[10] L. Wang, Y. Qi, Y. Wei, D. Fang, S. Meng, Z. Liu, Catal. Lett. 106 (2006) 61-66.

[11] D. Mao, W. Yang, J. Xia, B. Zhang, Q. Song, Q. Chen, J. Catal. 230 (2005) 140-149.

[12] P.S.S. Prasad, J.W. Bae, S.-H. Kang, Y.-J. Lee, K.-W. Jun, Fuel Process. Technol. 89 (2008) 1281-1286.

[13] A. García-Trenco, S. Valencia, A. Martínez, Appl. Catal. A 468 (2013) 102-111.

[14] R. Ahmad, D. Schrempp, S. Behrens, J.Sauer, M. Doering, U. Arnold, Fuel Process. Technol. 121 (2014) 38-46.

[15] J.W. Bae, S.-H. Kang, Y.-J. Lee, K.-W. Jun, J. Ind. Eng. Chem. 15 (2009) 566-572.

[16] G. Yang, N. Tsubaki, J. Shamoto, Y. Yoneyama, Y. Zhang, J. Am. Chem. Soc. 132 (2010) 8129-8136.

[17] G. Yang, M. Thongkam, T. Vitidsant, Y. Yoneyama, Y. Tan, N. Tsubaki, Catal. Today 171 (2011) 229-235.

[18] R. Nie, H. Lei, S. Pan, L. Wang, J. Fei, Z. Hou, Fuel 96 (2012) 419-425.

[19] K.S. Yoo, J.-H. Kim, M.-J. Park, S.-J. Kim, O.-S. Joo, K.-D. Jung, Appl. Catal. A 330 (2007) 57-62.

[20] J. Ereña, J. Vicente, A.T. Aguayo, M. Olazar, J. Bilbao, A.G. Gayubo, Appl. Catal. B 142-143 (2013) 315-322.

[21] S.Wang, D. Mao, X. Guo, G. Wu, G. Lu, Catal. Commun. 10 (2009) 1367-1370.

[22] A. García-Trenco, A. Vidal-Moya, A. Martínez, Catal. Today 179 (2012) 43-51.

[23] S.P. Naik, H. Du, H. Wan, V. Bui, J.D. Miller, W.W. Zmierczak, Ind. Eng. Chem. Res. 47 (2008) 9791-9794.

[24] A. García-Trenco, A. Martínez, Appl. Catal. A 411-412 (2012) 170-179.

[25] A. García-Trenco, A. Martínez, Catal. Today 227 (2014) 144-153.

[26] M.T. Twigg, M.S. Spencer, Topics Catal. 22 (2003) 191-203.

[27] D. Zhao, Q. Huo, J. Feng, B.F. Chmelka, G.D. Stucky, J. Am. Chem. Soc. 120 (1998) 6024-6036.

[28] N. Brodie-Linder, R. Besse, F. Audonnet, S. LeCaer, J. Deschamps, M. Impéror-Clerc, C. Alba-Simionesco, Microp. Mesop. Mater. 132 (2010) 518-525.

[29] X. Guo, A. Yin, W.-L. Dai, K. Fan, Catal. Lett. 132 (2009) 22-27.

[30] A. García-Trenco, A. Martínez, Catal. Today 215 (2013) 152-161.

[31] I. Melian-Cabrera, M. Lopez-Granados, J.L.G. Fierro, J. Catal. 210 (2002) 273–284.

[32] G.C. Chinchen, C.M. Hay, H.D. Vandervell, K.C. Waugh, J. Catal. 103 (1987) 79-86.

[33] R.M. Dell, F.S. Stone, P.F. Tiley, Trans. Faraday Soc. 49 (1953) 195-201.

[34] E.K. Poels, D.S. Brands, Appl. Catal. A 191 (2000) 83-96.

[35] D.S. Brands, E.K. Poels, T.A. Krieger, O.V. Makarova, Catal. Lett. 36 (1996) 175-182.

[36] J. Nakamura, T. Uchijima, Y. Kanai, T. Fujitani, Catal. Today 28 (1996) 223-230.

[37] O.P. Tkachenko, K.V. Klementiev, E. Löffler, I. Ritzkopf, F. Schüth, M. Bandyopadhyay, S. Grabowski, H. Gies, V. Hagen, M. Muhler, L. Lu, R.A. Fischer, W. Grünert, Phys. Chem. Chem. Phys. 5 (2003) 4325-4334.

[38] H. Gies, S. Grabowski, M. Bandyopadhyay, W. Grünert, O.P. Tkachenko, K.V. Klementiev, A. Birkner, Microp. Mesop. Mater. 60 (2003) 31-42.

[39] E.D. Batyrev, J.C. van den Heuvel, J. Beckers, W.P.A. Jansen, H.L. Castricum, J. Catal. 229 (2005) 136-143.

[40] C. Baltes, S. Vukojevic, F. Schüth, J. Catal. 258 (2008) 334-344.

[41] G.C. Chinchen, K.C. Waugh, D.A. Whan, Appl. Catal. A 25 (1986) 101-107.

[42] W.X. Pan, R. Cao, D.L. Roberts, G.L. Griffin, J. Catal. 114 (1988) 440-446.

[43] J.Nakamura, I. Nakamura, T. Uchijima, Y. Kanai, T. Watanabe, N. Saito, T. Fujitani, J. Catal. 160 (1996) 65-75.

[44] K. Klier, Adv. Catal. 31 (1982) 243-313.

[45] R.G. Herman, K. Klier, G.W. Simmons, B.P. Finn, J.B. Bulko, T.P. Kobylinski, J. Catal. 56 (1979) 407-429.

[46] G.R. Sheffer, T.S. King, J. Catal. 116 (1989) 488-497.

[47] J. Szanyi, D.W. Goodman, Catal. Lett. 10 (1991) 383-390.

[48] T. Fujitani, J. Nakamura, Appl. Catal. A 191 (2000) 111-129.

[49] M. Behrens, F. Studt, I. Kasatkin, S. Kühl, M. Häcecker, F. Abild-Pedersen, S. Zander, F. Girgsdies, P. Kurr, B.-L. Kniep, M. Tovar, R.W. Fischer, J.K. Nørskov, R.Schlögl, Science 336 (2012) 893-897.

[50] M.W.E. van den Berg, S. Polarz, O.P. Tkachenko, K.V. Klementiev, M. Bandyopadhyay, L. Khodeir, H. Gies, M. Muhler, W. Grünert, J. Catal. 241 (2006) 446-455.

[51] T. Fujitani, M. Saito, Y. Kanai, T. Kakumoto, T. Watanabe, J. Nakamura, T. Uchijima, Catal. Lett. 25 (1994) 271-276.

[52] J.-D. Grunwaldt, A.M. Molenbroek, N.-Y. Topsøe, H.Topsøe, B.S. Clausen, J. Catal. 194 (2000) 452-460.

[53] J. Greeley, A.A. Gokhale, J. Kreuser, J.A. Dumesic, H. Topsøe, N.-Y. Topsøe, M. Mavrikakis, J. Catal.213 (2003) 63-72.

[54] Y. Luan, H. Xu, C. Yu, W. Li, S. Hou, Catal. Lett. 125 (2008) 271-276.

[55] Y. Luan, H. Xu, C. Yu, W. Li, S. Hou, Catal. Lett. 115 (2007) 23-26.

[56] R. Montesano, D. Chadwick, Catal. Comm. 29 (2012) 137-140.

[57] M.S. Spencer, Top. Catal. 8 (1999) 259-266.

[58] J. Ereña, I. Sierra, M. Olazar, A.G. Gayubo, A.T. Aguayo, Ind. Eng. Chem. Res. 47 (2008) 2238–2247.

[59] A.T. Aguayo, J. Ereña, I. Sierra, M. Olazar, J. Bilbao, Catal. Today 106 (2005) 265–270.

[60] J.T. Sun, I.S. Metcalfe, M. Sahibzada, Ind. Eng. Chem. Res. 38 (1999) 3868-3872.

Table 1. Chemical composition and textural properties of S15, Zn@S15 and *x*Cu/Zn@S15 samples.

Sample	ICP-OES		N_2 physisorption			N_2O-RFC
	Cu (wt%)	Zn (wt%)	B.E.T. (m^2/g)	MPV[a] (cm^3/g)	Plugged mesopores[b]	Cu^0 area (m^2/g_{cat})
S15	-	-	771	0.93	-	-
Zn@S15	-	16.9	491	0.66	10	-
10Cu/Zn@S15	9.8	15.8	328	0.49	22	5.7 (58.2)
15Cu/Zn@S15	14.6	15.2	285	0.49	16	8.7 (59.6)
20Cu/Zn@S15	19.8	14.6	262	0.44	17	5.4 (27.3)

[a] Mesopore volume.

[b] Percentage of plugged mesopores in SBA-15 taking into account the mass-dilution effect by the supported CuO and ZnO phases and assuming preservation of the SBA-15 pore structure upon impregnation and calcination (see text).

[c] Values in parenthesis are the Cu^0 surface areas normalized per mass of Cu (m^2/g_{Cu}).

Table 2. Catalytic results for methanol synthesis on *x*Cu/Zn@S15 catalysts[a].

Catalyst	GHSV ($cm^3_{syngas}/(g_{cat}\cdot h)$)	MeOH synthesis rate ($mmol/(g_{cat}\cdot h)$)		Selectivity (%C)		
				MeOH	CO_2	Others[d]
		Initial[b]	Steady state[c]			
10Cu/Zn@S15	1873	2.47	1.65	91.5	2.5	6.0
15Cu/Zn@S15	6243	8.22	5.31	94.3	2.4	3.3
20Cu/Zn@S15	3390	4.29	2.91	94.8	1.6	3.6

[a] Reaction conditions: T= 533 K, P= 4.0 MPa, syngas composition (vol%): 66%H_2/30%CO/4%CO_2. The space velocity (referred to syngas) was adjusted in each case to obtain initial CO conversions of ca. 10%.
[b] Extrapolated at TOS= 0 from the rate-TOS curves (see Fig. S2b).
[c] At TOS~ 9 h.
[d] C_1-C_5 hydrocarbons, C_{2+} alcohols, and DME.

Table 3. Deactivation of hybrid catalysts during DME synthesis and properties of spent catalysts[a].

Catalyst	Relative loss of CO conversion (%)	Cu^0 surface area (m^2/g_{cu})	Relative loss of Cu^0 area (%)	Carbon content (wt%)
15Cu/Zn@S15+Z5(M)	10.8	53.9	9.5	0.6
CZA+Z5(M)	16.7	18.8	19.3	1.2
15Cu/Zn@S15+Z5(G)	11.1	51.0	12.2	0.8
CZA+Z5(G)	26.7	18.6	17.0	1.0

[a] Reaction conditions: T= 533 K, P= 4.0 MPa, and GHSV= 3710 and 4640 $cm^3_{syngas}/(g_{Cu}\cdot h)$ for the catalysts based on 15Cu/Zn@S15 and CZA, respectively. Feed composition: 90 vol% syngas (66 vol% H_2, 30 vol% CO, 4 vol% CO_2) + 10 vol% Ar (reference gas for GC analyses).

Figure captions

Figure 1. a) Nitrogen adsorption-desorption isotherms recorded at 77 K and b) pore size distributions for the calcined SBA-15 silica (S15), the SBA-15 silica coated with a monolayer of ZnO (Zn@S15), and the calcined Cu/Zn@S15 catalysts containing different amounts of copper (10, 15, and 20 wt%). The isotherms have been up-shifted by 150 (15Cu/Zn@S15), 300 (10Cu/Zn@S15), 450 (Zn@S15), and 550 (S15) cm^3/g for the sake of clarity.

Figure 2. a) Low-angle XRD patterns for the calcined SBA-15 silica (S15), the Zn@S15 composite, and the 15Cu/Zn@S15 calcined precursor; b) high-angle XRD patterns for the Zn@S15 composite and calcined *x*Cu/Zn@S15 catalysts with different Cu loadings.

Figure 3. H_2-TPR profiles for the calcined *x*Cu/Zn@S15 catalyst precursors.

Figure 4. Electron microscopy characterization of the 15Cu/Zn@S15 sample after reduction in flowing H_2 at 750 K: a) representative HAADF-STEM image evidencing a partial filling of the SBA-15 mesopores by confined metal phases; b) HRTEM image showing the presence of very small Cu^0 nanoparticles sizing 5-6 nm; c) HAADF-STEM (left) and EDX line profile analysis (right) collected along the white line in the HAADF-STEM image showing the confinement of copper within the SBA-15 silica walls.

Figure 5. CO conversion rate (per mass of copper) as a function of TOS in direct DME synthesis over the 15Cu/Zn@S15+Z5 and CZA+Z5 hybrid catalysts. Reaction conditions: T= 533 K, P= 4.0 MPa, and GHSV= 3710 and 4640 $cm^3_{syngas}/(g_{Cu}\cdot h)$ for the catalysts based on 15Cu/Zn@S15 and CZA, respectively. Feed composition: 90 vol% syngas (66 vol% H_2, 30 vol% CO, 4 vol% CO_2) + 10 vol% Ar (reference gas for GC analyses).

Figure 6. Normalized CO conversion during direct DME synthesis experiments for the 15Cu/Zn@S15+Z5 and CZA+Z5 hybrid catalysts as a function of time-on-stream (TOS). Reaction conditions: T= 533 K, P= 4.0 MPa, and GHSV= 3710 and 4640 $cm^3_{syngas}/(g_{Cu}\cdot h)$ for the catalysts based on 15Cu/Zn@S15 and CZA, respectively. Feed composition: 90 vol% syngas (66 vol% H_2, 30 vol% CO, 4 vol% CO_2) + 10 vol% Ar (reference gas for GC analyses).

Supplementary Material

for

A rational strategy for preparing Cu-ZnO/H-ZSM-5 hybrid catalysts with extended lifetime during the one-step conversion of syngas to dimethyl ether (DME)

Andrés García-Trenco, Agustín Martínez

Table S1. Main physicochemical properties of the reference coprecipitated Cu-ZnO-Al_2O_3 (CZA) methanol synthesis catalyst.

Cu/Zn/Al atomic ratio		BET area	T_{max}[b] (H_2-TPR)	d_{CuO}[c]	Cu^0 area[d]	
Nominal	Experimental[a]	(m^2/g)	(K)	(nm)	(m^2/g_{cat})	(m^2/g_{Cu})
55/30/15	57/29/14	43	453	8.3	11.1	23.3

[a] From ICP-OES. The experimental Cu content in the calcined catalyst is 52.6 wt%.

[b] Temperature of maximum H_2 consumption from H_2-TPR.

[c] Average diameter of CuO crystallites in the calcined precursor estimated from XRD by applying the Scherrer's equation.

[d] Metallic copper area measured by N_2O-RFC.

Fig. S1. FTIR spectra (normalized by mass of sample) in the OH stretching region for the SBA-15 silica matrix (S15) and ZnO_x@SBA-15 composite (Zn@S15).

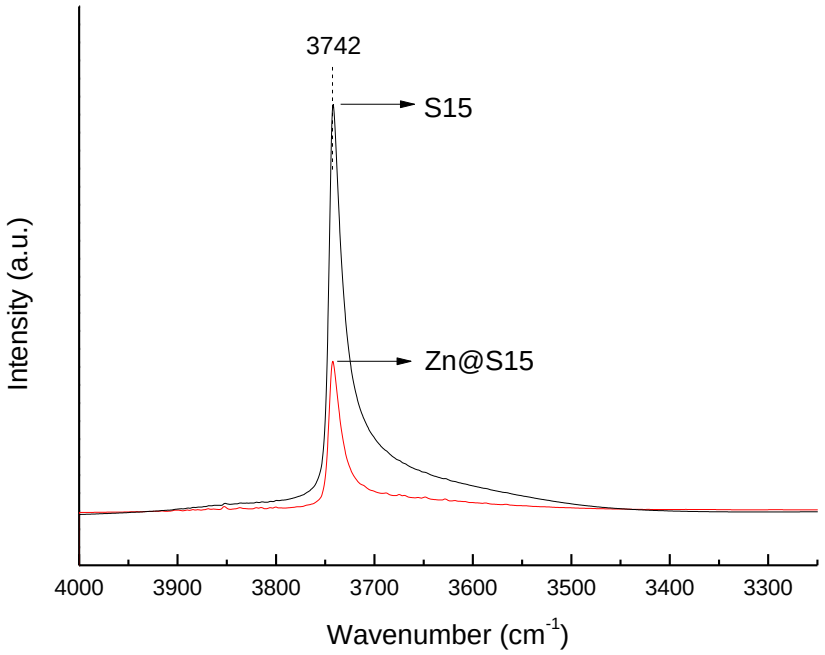

Fig. S2. CO conversion (a) and methanol synthesis rate (b) as a function of TOS for the xCu/Zn@S15 catalysts. Reaction conditions: T= 533 K, P= 4.0 MPa, GHSV values adjusted to obtain initial CO conversions of ca. 10% (GHSV= 1873, 6243, and 3390 $cm^3_{syngas}/(g_{cat}\cdot h)$ for catalysts loaded with 10, 15, and 20 wt% Cu, respectively), syngas composition (vol%): 66%H_2/30%CO/4%CO_2.

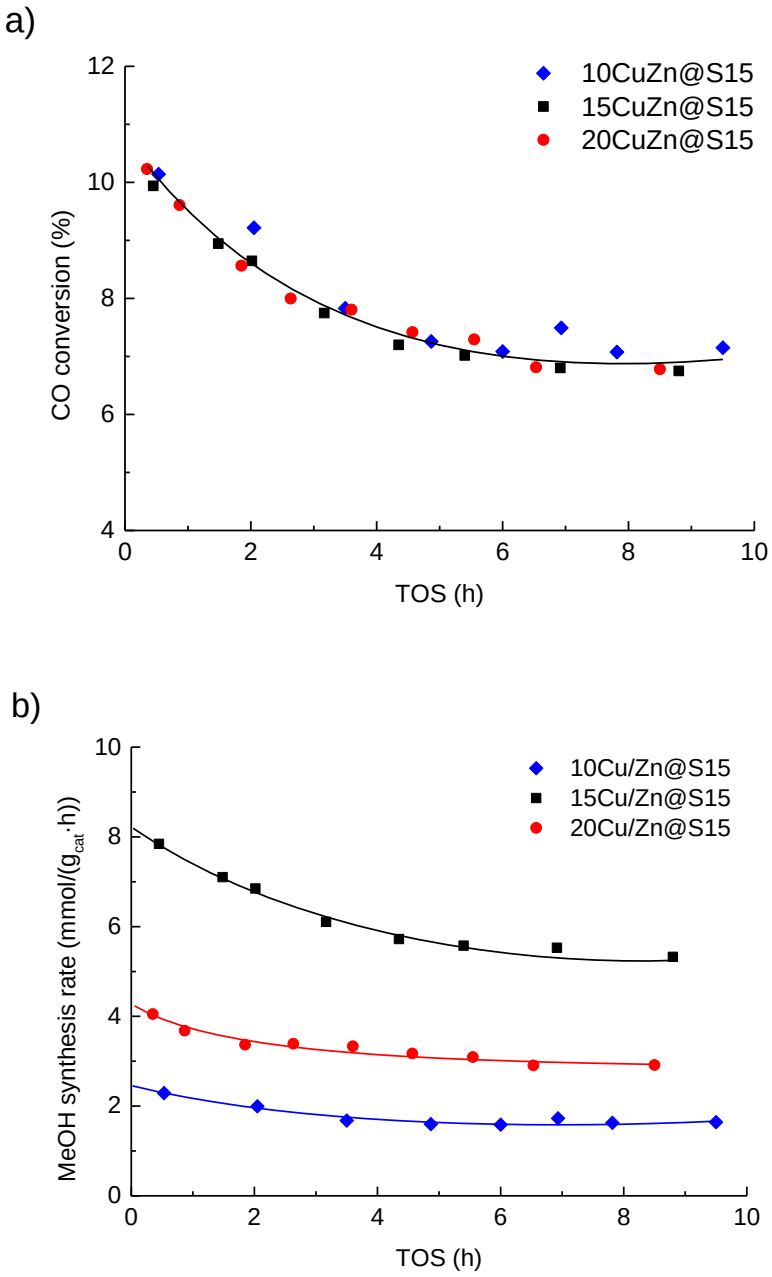

Fig. S3. CO conversion (a) and DME selectivity (b) as a function of TOS for the 15Cu/Zn@S15+Z5 and CZA+Z5 hybrid catalysts prepared by mixing (M) and grinding (G) methods. Reaction conditions: T= 533 K, P= 4.0 MPa, and GHSV= 3710 and 4640 $cm^3_{syngas}/(g_{Cu} \cdot h)$ for the catalysts based on 15Cu/Zn@S15 and CZA, respectively. Feed composition: 90 vol% syngas (66 vol% H_2, 30 vol% CO, 4 vol% CO_2) + 10 vol% Ar (reference gas for GC analyses).

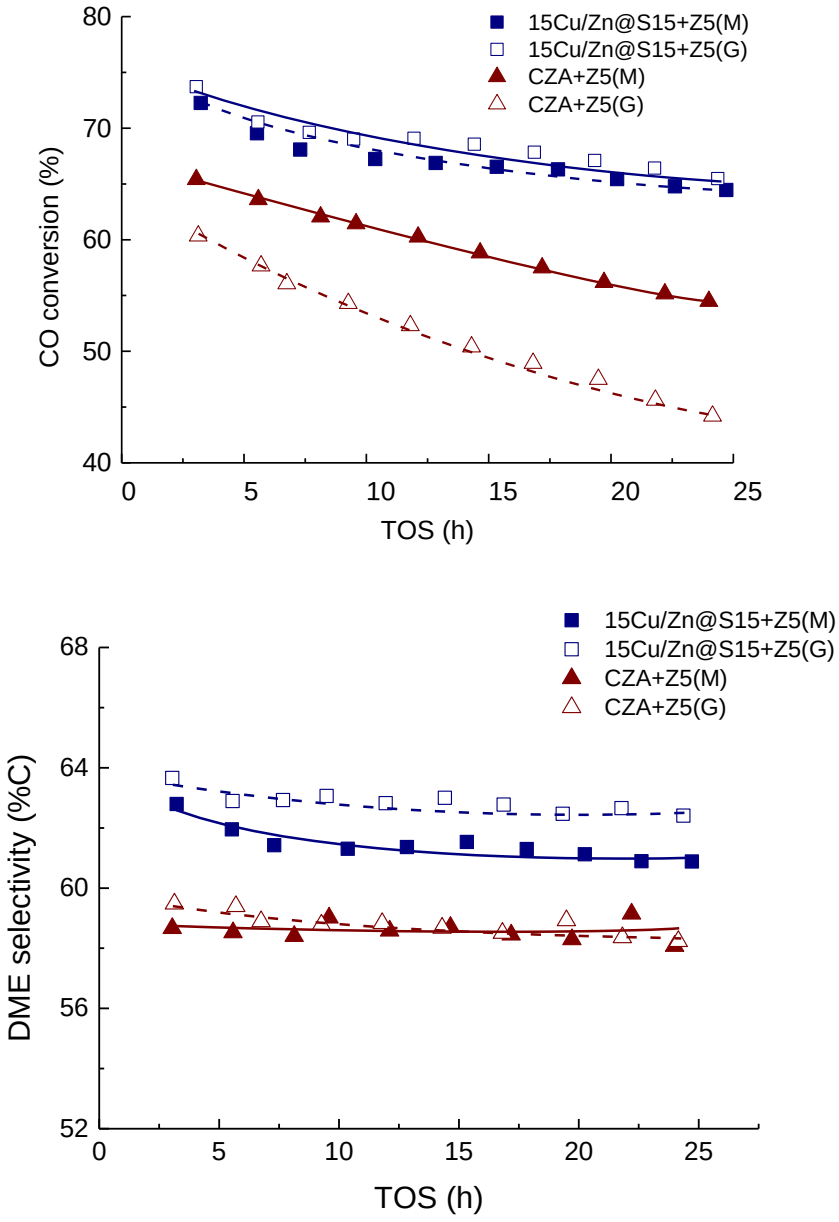

Fig. S4. Temperature-programmed oxidation (TPO) experiments for the hybrid catalysts after their evaluation in the syngas-to-DME reaction during ca. 24 h. The TPO profile for the calcined (*fresh*) CZA catalyst is also provided to support the assignation of the high-temperature oxidation peaks to the combustion of residual carbonates.

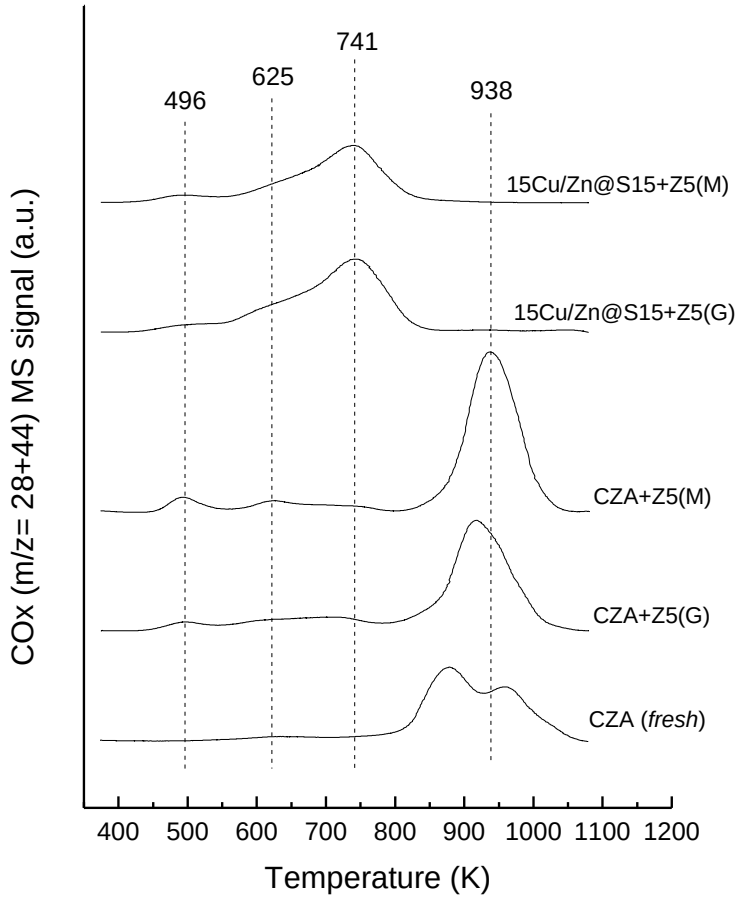

Fig. 1

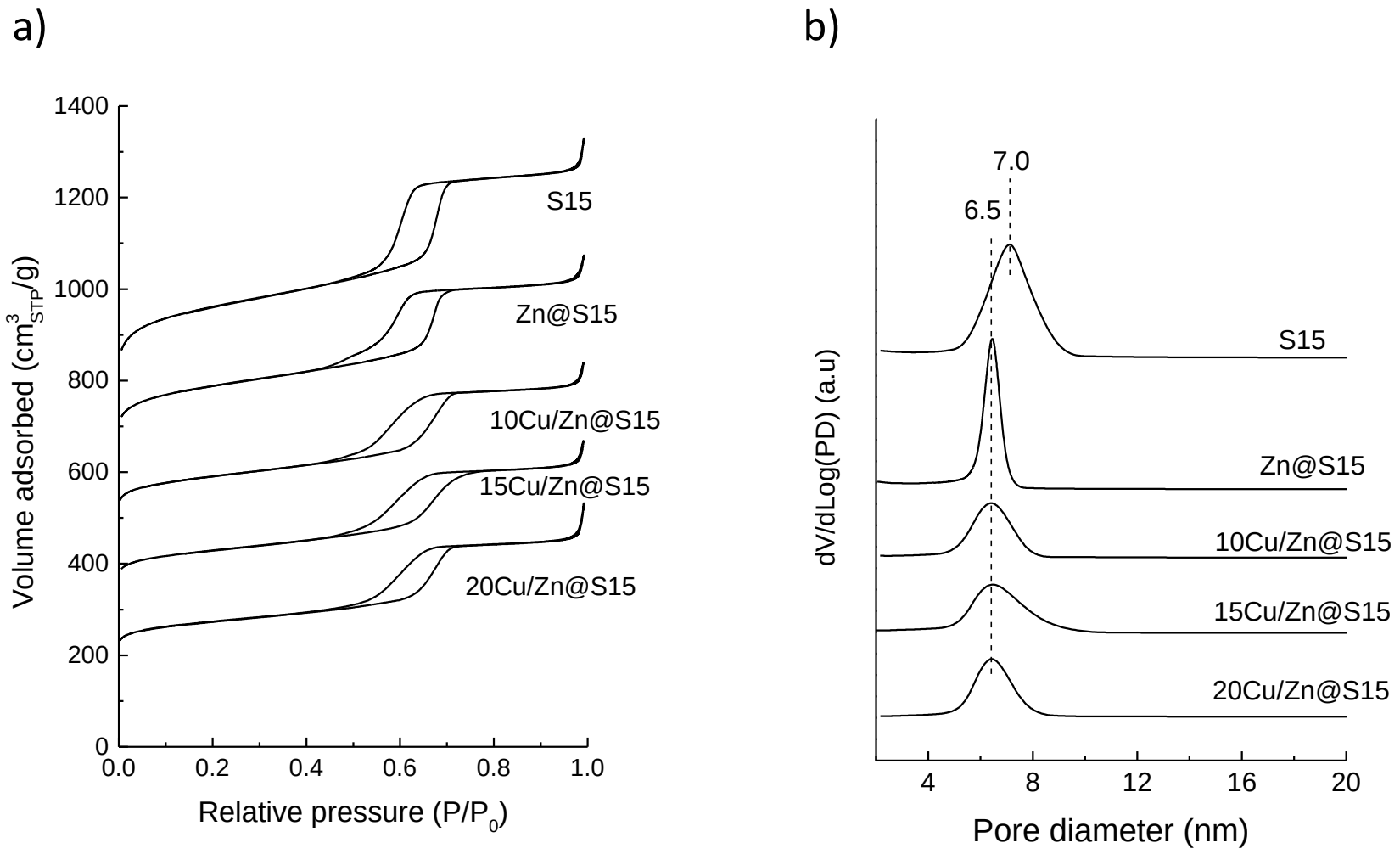
a)
b)
Volume adsorbed (cm^3_{STP}/g)
Relative pressure (P/P_0)
S15
Zn@S15
10Cu/Zn@S15
15Cu/Zn@S15
20Cu/Zn@S15
dV/dLog(PD) (a.u)
Pore diameter (nm)
7.0
6.5

Fig. 2

a)

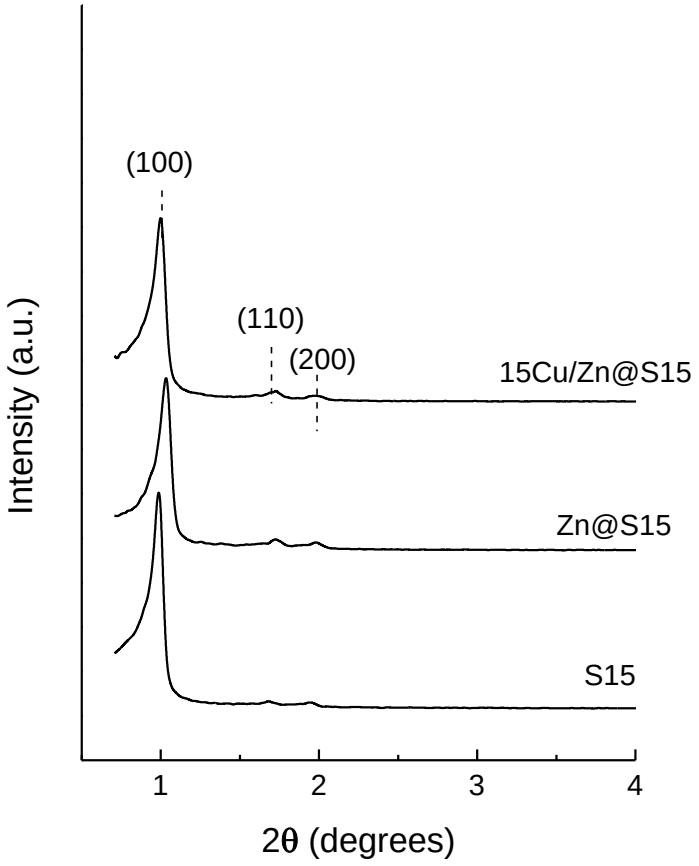
(100)
(110)
(200)
15Cu/Zn@S15
Zn@S15
S15
Intensity (a.u.)
1
2
3
4
2θ (degrees)

b)

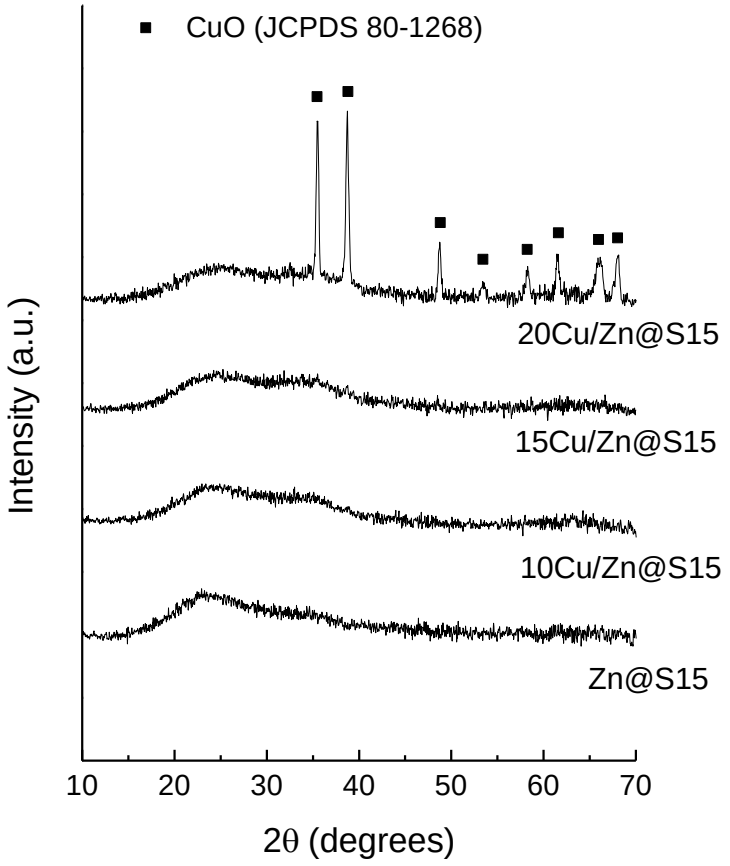
CuO (JCPDS 80-1268)
20Cu/Zn@S15
15Cu/Zn@S15
10Cu/Zn@S15
Zn@S15
Intensity (a.u.)
10
20
30
40
50
60
70
2θ (degrees)

Fig. 3

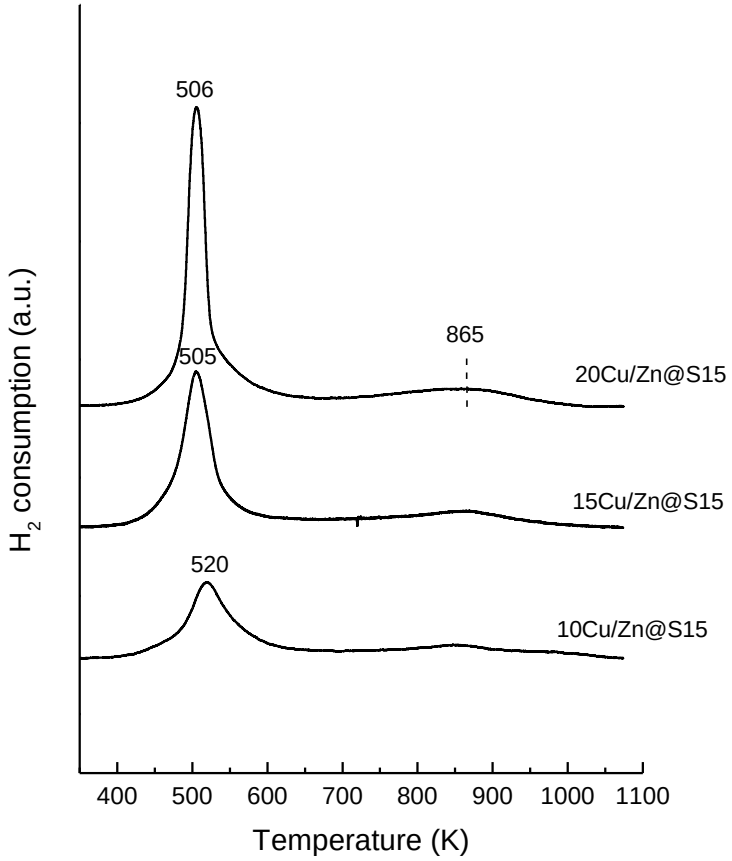
506
865
505
20Cu/Zn@S15
15Cu/Zn@S15
520
10Cu/Zn@S15
H2 consumption (a.u.)
400
500
600
700
800
900
1000
1100
Temperature (K)

Fig. 4

a)

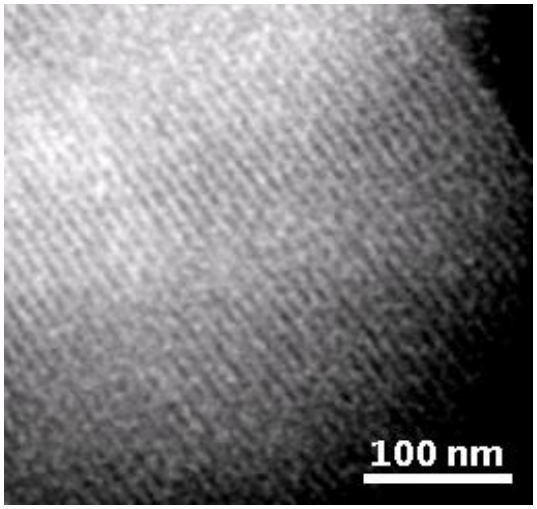
100 nm

b)

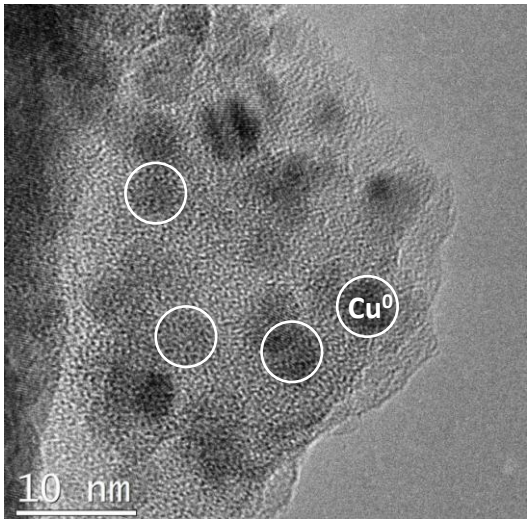
Cu0
10 nm

c)

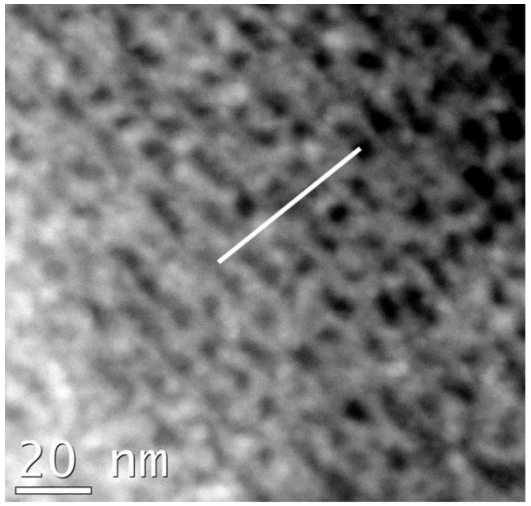
20 nm

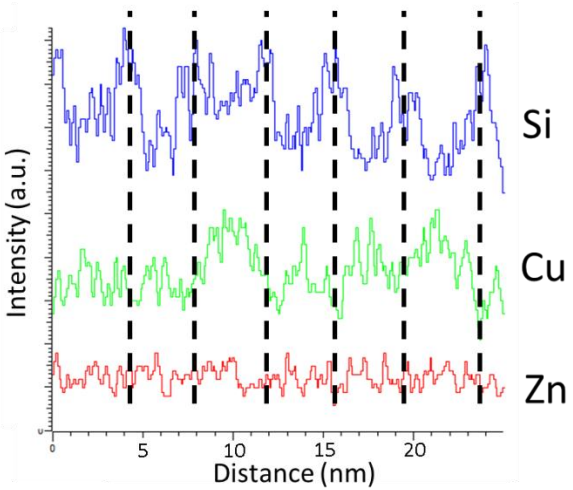
Intensity (a.u.)
Si
Cu
Zn
0
5
10
15
20
Distance (nm)

Fig. 5

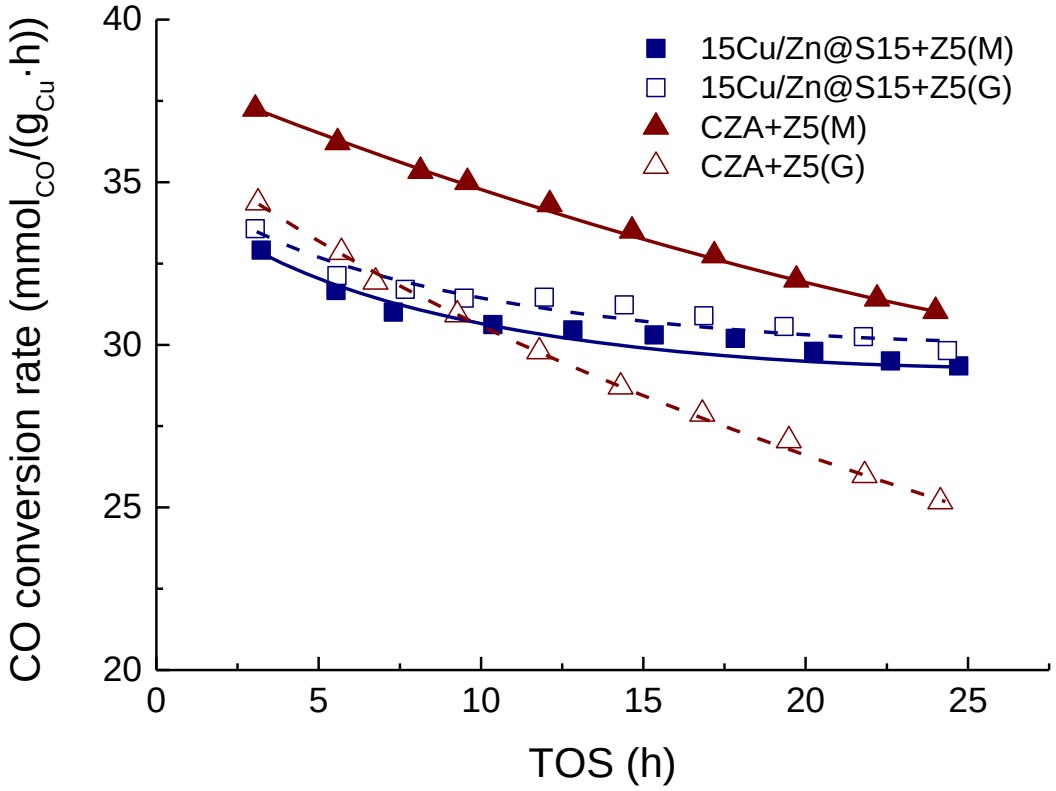
15Cu/Zn@S15+Z5(M)
15Cu/Zn@S15+Z5(G)
CZA+Z5(M)
CZA+Z5(G)
CO conversion rate (mmol$_{CO}$/(g$_{Cu}$·h))
TOS (h)
40
35
30
25
20
0
5
10
15
20
25

Fig. 6

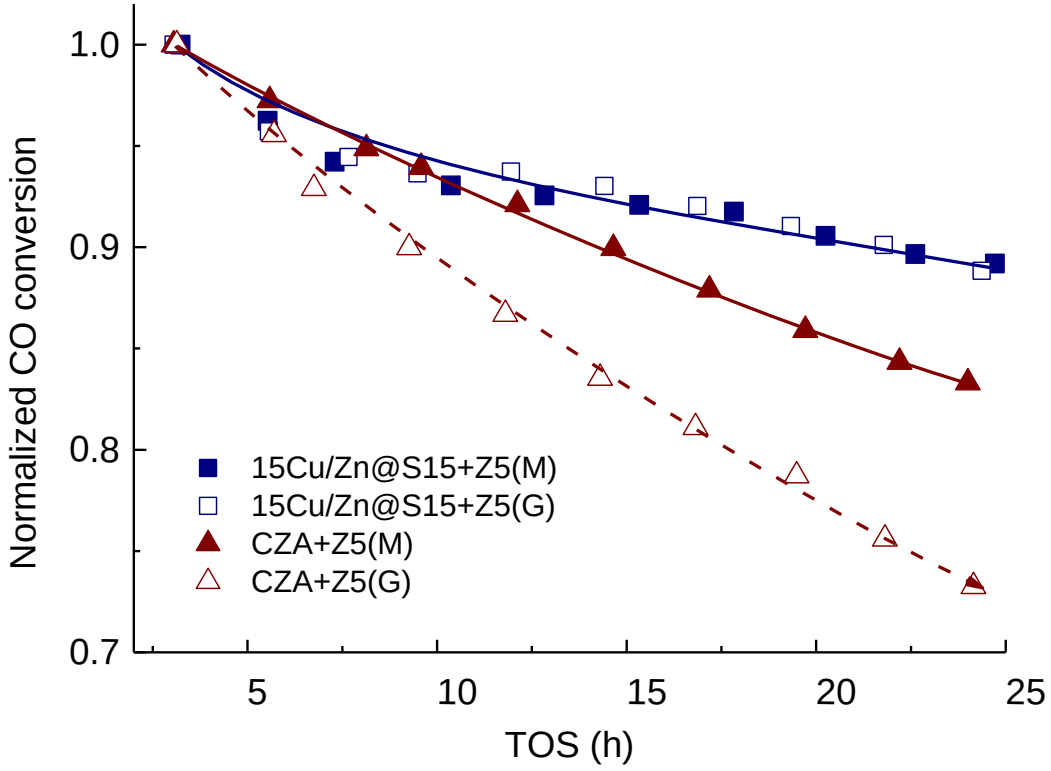
Normalized CO conversion
1.0
0.9
0.8
0.7
5
10
15
20
25
TOS (h)
15Cu/Zn@S15+Z5(M)
15Cu/Zn@S15+Z5(G)
CZA+Z5(M)
CZA+Z5(G)